PCCP

View Online
Dynamic Article Links

Cite this: DOI: 10.1039/c1cp21834d

www.rsc.org/pccp

PAPER

Water reorientation dynamics in the first hydration shells of F^- and I^-

Jean Boisson,†[a] Guillaume Stirnemann,[a] Damien Laage*[a] and James T. Hynes*[ab]

Received 7th June 2011, Accepted 24th August 2011
DOI: 10.1039/c1cp21834d

Molecular dynamics and analytic theory results are presented for the reorientation dynamics of first hydration shell water molecules around fluoride and iodide anions. These ions represent the extremes of the (normal) halide series in terms of their size and conventional structure-making and -breaking categorizations. The simulated reorientation times are consistent with NMR and ultrafast IR experimental results. They are also in good agreement with the theoretical predictions of the analytic Extended Jump Model. Analysis through this model shows that while sudden, large amplitude jumps (in which the reorienting water exchanges hydrogen-bond partners) are the dominant reorientation pathway for the I^- case, they are comparatively less important for the F^- case. In particular, the diffusive reorientation of an intact $F^-\cdots H_2O$ hydrogen-bonded pair is found to be most important for the reorientation time, a feature related to the greater hydrogen-bond strength for the $F^-\cdots H_2O$ pair. The dominance of this effect for *e.g.* multiply charged ions is suggested.

1. Introduction

The first hydration shell dynamics for anions, beyond its fundamental interest in connection with hydrogen-bond (H-bond) dynamics,[1,2] is important in many contexts, ranging from chemical reactions in aqueous solution,[3,4] at aqueous surfaces important for the atmosphere[5,6] and at electrode–ionic solution interfaces,[7] to the mobility and other transport properties of these ions in aqueous media.[1,2] Accordingly, much experimental effort has been directed towards elucidating these dynamics, especially *via* NMR,[8–10] and most recently by investigation *via* femtosecond infrared (fsIR) pump–probe and photon-echo spectroscopies,[11–15] coherent Raman scattering[16] and THz spectroscopy.[17]

Here we extend the previous work of two of us on the chloride anion in aqueous solution[18] to examine the first hydration shell dynamics for the fluoride and iodide ions.[19,20] The F^- and I^- anions represent extremes in the halide series, in the sense that the small F^- anion is regarded as a fairly strong structure maker,[2,21] while the considerably larger I^- anion is considered a modest structure breaker.[2,21] However, as has been stressed *e.g.* by Soper and coworkers,[21,22] these terms can be rather ambiguous from a structural perspective. We employ instead a dynamical criterion for these designations,[8,9] *i.e.* whether the reorientation time for a water molecule in the anion's first hydration shell is larger or smaller, respectively, than the corresponding time for a water molecule in bulk water. As with other measures, this criterion will have its limitations, but does have the merit of connecting to an increasing number of modern spectroscopic investigations.[11–17] We will focus on τ_2, the (second-order) reorientation time connected to NMR and fsIR experiments, and compare our values calculated both by Molecular Dynamics (MD) simulation and by application of the analytic Extended Jump Model,[23,24] previously shown to be a good description for the reorientation dynamics of water around the chloride ion[18] and next to a very wide range of other solutes.[25–28]

The outline of the remainder of the paper is as follows. In Section 2, we describe the polarizable potentials employed and some structural characteristics for the ions such as radial distribution functions and coordination numbers. Section 3 is devoted to MD results for τ_2 and for the time correlation function from which it is determined, including an examination of the reorientational slowdown or speedup compared to the neat water value, a dynamical characterization of structure-making and -breaking characters, respectively. Comparison is also made with NMR and fsIR experiments, which involves a discussion of some key assumptions employed in the experimental extraction of τ_2. The theoretical analysis of the results is presented in Section 4, including the justification and application of the Extended Jump Model[23,24] (which reveals the quite special character of the water reorientation for the F^- anion). Concluding remarks are offered in Section 5.

2. Methodology and potentials of mean force

Simulations and potentials

In this section, we describe the potentials employed and the calculated radial distribution functions $g(r)$ and first hydration shell coordination numbers n for the anions and water.

[a] *Ecole Normale Supérieure, Chemistry Department, UMR CNRS-ENS-UPMC 8640, 24 rue Lhomond, 75005 Paris, France. E-mail: damien.laage@ens.fr, hynes@spot.colorado.edu*
[b] *Department of Chemistry and Biochemistry, University of Colorado, Boulder, CO 80309-0215, USA*
† Current address: DSM/SPEC/IRAMIS/CEA Saclay and CNRS (URA 2464), 91191 Gif-sur-Yvette Cedex, France.

The latter are compared with literature experimental results for calibration purposes; much experimental information for aqueous solutions of these anions is available,[1,9,21,29,30] as are previous simulation results.[31–34]

The importance of the utilization of polarizable potentials for ionic systems has been emphasized earlier.[35,36] Here, one anticipates that the water polarizability is especially important for the small F^- anion, while the anion polarizability is key for the large I^- ion. Our simulations employ the polarizable Amoeba potentials for all species.[37,38]

For each anion case, MD simulations at the experimental bulk water density were performed with Amber 10[39] with 499 water molecules and 1 anion in a cubic simulation box of side 24.625 Å with periodic boundary conditions, using Ewald summation.[40] In the pure water simulations, the anion was replaced with an H_2O. The simulations were each of duration 1 ns, with a 1 fs time step. They commenced with an equilibration period of at least 200 ps at 298 K, followed by a production run in the canonical ensemble using Langevin dynamics with a collision frequency of 0.5 ps^{-1}, which we verified not to induce any dynamical artefact. A configuration was selected every 100 fs from this trajectory.

Hydration shells

The calculated radial distribution functions (rdf) $g(r_{XO})$ (where X is the anion or "solute" water oxygen and O represents a water oxygen) and the corresponding coordination numbers n for the two anion and pure water cases are displayed in Fig. 1. The coordination number n is defined as the value of the integrated $g(r)$ at the first minimum of the rdf. For our purposes, the key features are as follows. For the F^- case, the large and sharp initial peak at 2.9 Å indicates a well-defined first hydration shell with $n = 5.8$. In contrast, for the larger I^- the considerably lower first peak at 3.85 Å with its rather broad character depicts a more diffuse first hydration shell, leading to $n = 6.7$ when the shell radius value is taken to be 4.10 Å as experimentally determined in ref. 21. These results are in reasonable agreement with X-ray diffraction[1] and neutron scattering,[21] as well as with previous mixed quantum/classical simulations[34,41] (*cf.* Table 1).

Table 1 Structural properties of the first hydration layer for fluoride and iodide ions

		F^-	I^-
First peak position r_{XO}/Å	This work	2.78	3.64
	Expt[21]	2.54	3.63
	Expt[1]	2.62–2.92	3.54–3.7
	Previous simulations[34,41]	2.53–2.68	3.45–3.71
Coordination number n	This work	6.0	6.7
	Expt[21]	6.9	6.7
	Expt[1]	4–6	4.2–9.6
	Previous simulations[34,41]	4.6–6.0	6.6–9.7

3. Water reorientation times

We extract the reorientation time τ_2 values from MD simulations of the second-order Legendre polynomial equilibrium time correlation function (tcf)

$$C_2(t) = \langle P_2\,[\mathbf{u}(0)\cdot\mathbf{u}(t)]\rangle, \qquad (1)$$

where we take $\mathbf{u}$ to be the unit vector of a water OH, the appropriate choice for fsIR measurements[11–15] (some comment is given later concerning the different vectors relevant for the NMR measurements). These tcfs are displayed in Fig. 2, respectively, for a water OH in the bulk and initially H-bonded to F^- and I^- anions. All display the standard features of a rapid (sub-ps) initial librational decay, followed by a slower (ps) exponential decay. Our tabulated τ_2 values in Table 2 are extracted from the latter decays. We note at this stage that the reorientation time for water initially in F^-'s first hydration shell is about twice that for those in the I^- case and for pure water, which are very close to each other. This clearly indicates (from a dynamical perspective) the pronounced structure-making character of F^-. The reorientation times computed for a water molecule OH initially in the ion's second shell show that the dynamical influence of these two ions does not extend significantly beyond the first shell.

The simulated reorientation times are compared with values determined from NMR[42] and from fsIR experiments[30] in Table 2.

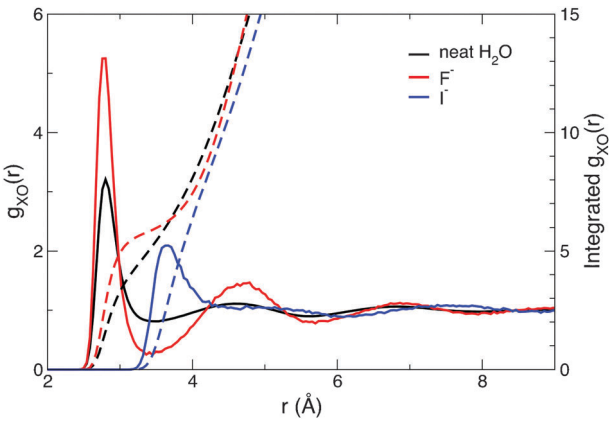

Fig. 1 Radial distribution functions $g(r_{XO})$ (solid lines) and integrated rdf (dashed lines) for water in the bulk and around F^- and I^- anions.

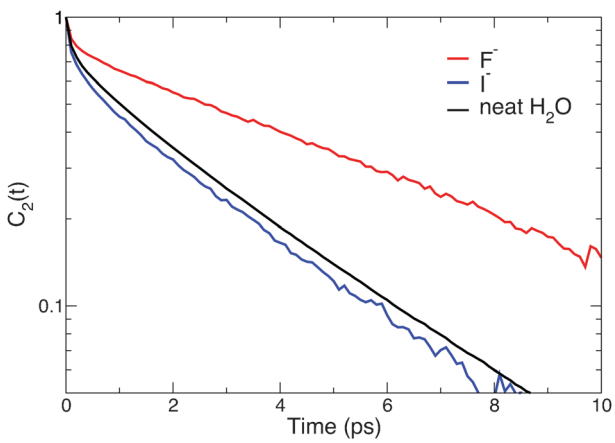

Fig. 2 Orientation time correlation functions $C_2(t)$ (eqn (1)) for the OH bond of a water molecule initially hydrogen-bonded to F^-, I^-, and H_2O, respectively.

Table 2 Second-order reorientation times (in ps), respectively from the MD simulations for a water OH initially H-bonded to an ion (or a water), and the anion's second shell, NMR and MD B values, and reorientation times from fsIR experiments, together with the MD determination including the vibrational lifetime effect[a]

	F^-	I^-	H_2O
τ_2/ps[b]	6.1	3.3	3.4
τ_2^{∞}/ps[c]	4.6	2.2	2.2
$\tau_2^{\text{2nd shell}}$/ps	3.5	3.2	—
B_{OH}^{MD}/kg/mol	0.12	−0.01	—
B_{H}^{NMR}/kg mol^{-1} [8]	0.14	−0.08	—
$B_{^{17}O}^{NMR}$/kg mol^{-1} (D_2O)[10,42]	0.114–0.129	−0.063–−0.055	—
$B_{^2H}^{NMR}$/kg mol^{-1} (D_2O)[42]	0.109	−0.066	—
$\tau_2^{fsIR,MD}$/ps	—	7.1	3.4
τ_2^{fsIR} [30]/ps (D_2O)	—	7.5	3.0

[a] Unless otherwise specified, the reported quantities were measured in H_2O. [b] Computed from the exponential tail of MD $C_2(t)$ on the 2–10 ps interval. [c] Computed from the full time integral of the MD $C_2(t)$.

For each type of experiment, we need to provide some commentary to understand the comparisons.

Comparison with NMR

NMR experiments provide information on the reorientation dynamics through measurement of the spin-lattice relaxation rate R_1, which is partly determined by orientational relaxation.[43–47] However, NMR is not sufficiently time-resolved to follow the water dynamics in the time domain; the inferred (but not directly measured) relaxation time is the orientational tcf time integral,

$$\tau_2^{\infty} = \int_0^{\infty} C_2(t)\mathrm{d}t = \int_0^{\infty} \langle \mathrm{P}_2[\mathbf{u}(0)\cdot\mathbf{u}(t)]\rangle \mathrm{d}t, \qquad (2)$$

where $C_2(t)$ is the second-order correlation function (eqn (1)) of a molecular vector. As discussed below in more detail, different NMR techniques probe reorientation of different molecular vectors, which are distinct but connected to the OH vector, a feature not accounted for in the notation of eqn (2). The fact that only an average integrated time is accessible has two important consequences. First, the resulting τ_2^{∞} value thus includes the short-time librational contribution mentioned above in addition to the longer time exponential contribution we have used to define τ_2. Thus τ_2^{∞} is smaller than τ_2, an effect which becomes more important as τ_2 decreases (see the comparison of τ_2 and τ_2^{∞} both calculated for the same initial H-bond conditions from the MD simulations and reported in Table 2). The second consequence is that the reorientation time measured by NMR is averaged over all the different environments that can be experienced by a water OH; the resulting τ_2^{∞} is therefore a weighted average of the reorientation times of the different mechanisms (*e.g.* with a water or anion initial H-bond acceptor).

NMR experiments thus isolate the influence of the solute for very dilute solutions, where the spin relaxation rate depends linearly on the solute molality[10,46,48,49] *via*

$$\frac{R_1^{\text{blk}}}{R_1} = \frac{\langle\tau_2\rangle}{\langle\tau_2^{\text{blk}}\rangle} = 1 + Bm, \qquad (3)$$

where R_1, R_1^{blk}, $\langle\tau_2\rangle$, $\langle\tau_2^{\text{blk}}\rangle$ are the spin relaxation rates and the average water reorientation times, respectively, for the entire solution at molality m (in mol kg^{-1}) and for bulk water, and where B is the proportionality factor of interest. Using the coordination number determined by other techniques (*e.g.* simulation or scattering), NMR studies then infer from B an average water reorientation retardation factor around the solute.[8]

To avoid the bias of assuming a coordination number, we directly compare our simulations with the NMR results through the B proportionality factors. To determine the B factor for the OH reorientation from our simulations, a virtual concentration study is performed on our single, dilute simulation box, as follows. We consider the average reorientation time of water molecules that lie in a sphere centered on the anion, and whose radius varies from a few Angströms (corresponding to the higher concentrations) to one-half of the simulation box (corresponding to the lower concentrations). We note that the critical region to determine B is the low-concentration/large-sphere domain, where the sphere boundary is far from the ion and where artefacts resulting from water molecules entering/leaving the sphere are very limited.

Results are displayed in Fig. 3, and the corresponding B^{MD} values are compared with the available NMR results in Table 2. Different isotopes have been used in the experiments, probing the reorientation of different molecular vectors: deuterium NMR in D_2O probes the OD bond reorientation, proton NMR in H_2O probes the HH intramolecular vector reorientation, and ^{17}O NMR probes the reorientation of the vector orthogonal to the molecular plane.[47,50,51] The different NMR results shown in Table 2 evidence two important points. First, since the reorientation times of the different molecular vectors are similar, the reorientation of water next to the F^- and I^- anions is only slightly anisotropic, as already shown for the bulk.[47] Second, while the absolute values of the reorientation times differ in H_2O and D_2O (at 298 K, τ_2^{∞} = 1.95 ps in H_2O[52] *vs.* 2.5 ps in D_2O,[10] and the long decay times measured by fsIR[53] are 2.5 ps and 3.0 ps, respectively), the relative slowdown/acceleration factors induced in the two solvents are similar (Table 2). In what follows, we will therefore

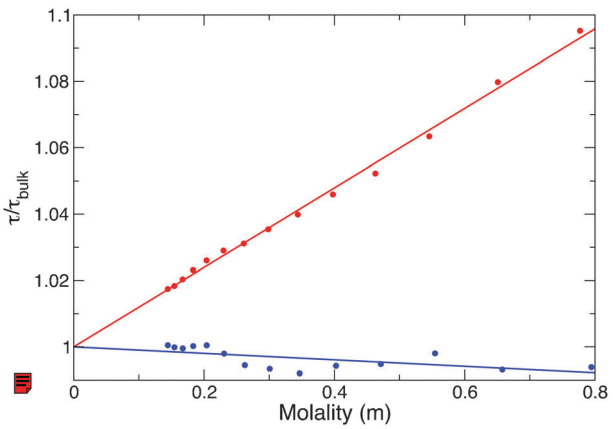

Fig. 3 The ratio of the fully integrated tcf reorientation time τ_2^{∞}, eqn (2), of water in the ionic solution (red for F^-, blue for I^-) and in the bulk *versus* molality. Straight lines are linear fits.

compare the slowdown/acceleration factors calculated from our simulations in H_2O solutions with the experimental results obtained for different isotopic situations.

The agreement between our computed B factors and the experimental determinations is excellent for the F^- case, where MD and NMR both depict F^- as a strong structure maker, while for the I^- case the agreement is only qualitative, both the MD and NMR results characterizing I^- as a weak structure breaker.

Comparison with fsIR

Finally, the reorientation time τ_2^{fsIR} is, in principle, the proper object for comparison with our τ_2 results, since it is obtained from the longer time orientational anisotropy, which is proportional to $C_2(t)$, eqn (1) (except at sub-ps delays where the relationship may be more complex). For present purposes, we emphasize only that the τ_2^{fsIR} values extracted in fsIR experiments for halide solutions involve the vibrational excitation of the water OH.[30] This requires that the vibrational population lifetime T_1 for a water molecule in the anion's hydration shell sufficiently exceeds that for a bulk water molecule such that a τ_2^{fsIR} appropriate for the shell can be extracted from the longer time anisotropy signal.[30] This requirement is not met for the F^- anion,[30] so that the reorientation time cannot be determined *via* this technique. This requirement is met for the I^- case;[30] however, T_1 considerations introduce[18] a bias in the determination which produces reorientation times longer than τ_2 (as is evident in Table 2); this will be further discussed in Section 4.

4. Theoretical analysis of water reorientation

Reorientation mechanism and the extended jump model

In previous work on neat water[23,24] and on the first hydration shell water molecules of Cl^- [18] and a variety of other solutes,[26,27] it has been shown that the dominant water reorientation mechanism is a sudden, large amplitude jump of the reorienting water OH between initial and final H-bond acceptors (for recent reviews, see ref. 54 and 55). Fig. 4 defines some of the key coordinates for the jump mechanism, considering a water molecule initially H-bonded to (in the present case) an anion. The H-bond exchange mechanism involves the concerted motions of the initial and the final H-bond partners. While the initial H-bond between a water OH* and the anion X^- elongates (increase of $R_{O^*X^-}$), the final partner O^f approaches the reorienting water molecule (decrease of $R_{O^*O^f}$). When the relative H-bond strengths of the initial and final partners of OH* are equal,[18,27] an angular jump of the OH* can occur, breaking the initial H-bond and forming a new H-bond. Here, we first demonstrate that such jumps occur for the F^- and I^- first hydration shell water molecules. We then show, *via* the analytic Extended Jump Model (EJM),[23,24] that while this H-bond-breaking and -making jump mechanism is indeed dominant for the I^- case, it is an important though not dominant contribution in the F^- case, where a previously identified mechanism of the reorientation of an intact H-bonded complex[23,24] is in fact more significant. Our simulation procedure for detecting and characterizing jumps has been described in detail elsewhere,[23,24] and the average trajectory data are shown in Fig. 5.

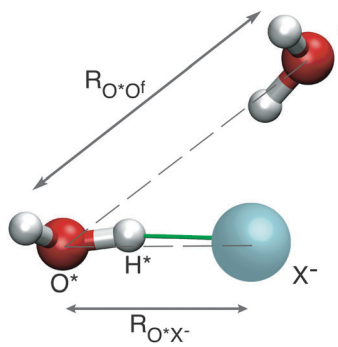

Fig. 4 Schematic figure depicting the key coordinates involved in the jump mechanism.

Within the analytic EJM framework, the reorientation time is given by[23,24]

$$\frac{1}{\tau_2} = \frac{1}{\tau_{jump}}\left[1 - \frac{\sin(5\Delta\theta/2)}{5\sin(\Delta\theta/2)}\right] + \frac{1}{\tau_{frame}}. \qquad (4)$$

The first term corresponds to the jump contribution to reorientation, due to Ivanov.[56] It only depends on two key ingredients, which are the jump angle $\Delta\theta$, determined from the simulations as an average over the successful jump trajectories, and the exchange time τ_{jump}, whose microscopic interpretation[23,24] is the

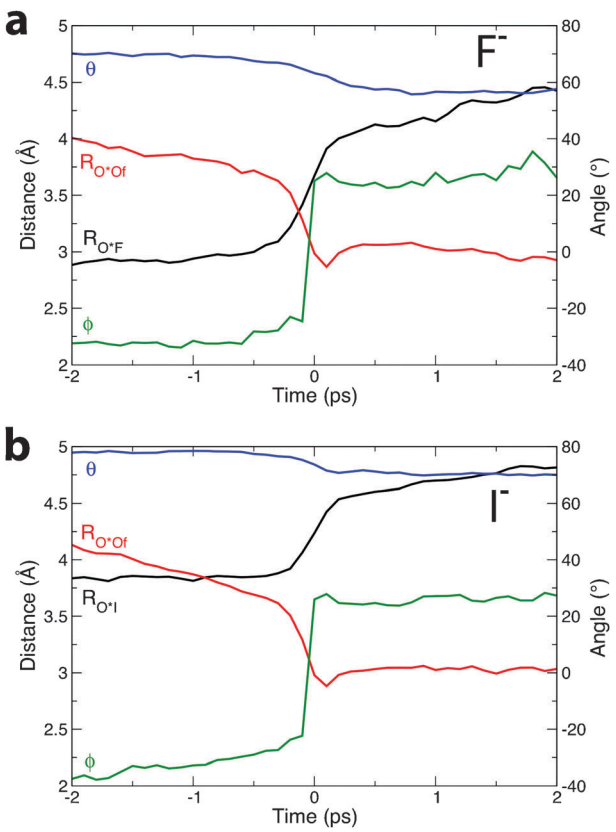

Fig. 5 Average trajectory results for the F^- and I^- cases for various coordinates characterizing the jump mechanism. See Fig. 4 for the distance coordinate definitions. For the angular coordinates, ϕ is the angle between the rotating, O*H* bond and the bisector plane of the XO^*O^f angle θ.

inverse of the rate constant for the jump, viewed as a chemical reaction. This is the (average) time to replace one stable H-bond by another one. Its evaluation employs the Stable States Picture of reactions,[24,57,58] which eliminates errors in the rate constant due to improper accounting of transition state recrossing effects; this requires a definition of the reactant and product regions for the reaction, which in line with previous work[24] is based on geometric criteria tighter than usual to define the H-bonds. Finally, τ_{frame} is the reorientation time of the O*–X axis, where X is the anion or a water oxygen, in an intact H-bonded complex, which is evaluated from the simulated trajectory portions between jump events. Eqn (4) predicts that the faster of two mechanisms will dominate the reorientation time when there is a large difference in magnitude between the individual times. Table 3 shows various characteristics for jump water reorientation for the F^- and I^- cases (with the neat water results also shown in the table). Included in the table are two versions of the EJM prediction for the reorientation time to be compared with the MD τ_2 values. The first of these is the average $\langle\tau_2^{\mathrm{EJM}}\rangle_{\Delta\theta}$ of eqn (4) over the jump trajectories (and their jump amplitudes), while the second, τ_2^{EJM} ($\langle\Delta\theta\rangle$), is eqn (4) evaluated at the average jump angle $\langle\Delta\theta\rangle$. The first of these should be considered more accurate since it more completely reflects the jump angle distribution; this accuracy, however, comes at the cost of some simplicity since the relationship between the reorientation times of successive orders (*e.g.* τ_2 and τ_1[23]—the latter, within strong approximations is related to the dielectric relaxation time) then depends on the jump angle distribution and not only on its average.

The agreement between the EJM predictions $\langle\tau_2^{\mathrm{EJM}}\rangle_{\Delta\theta}$ and the MD simulation results τ_2 in Table 3 is excellent for both F^- and neat H_2O. For I^-, the agreement appears to be only fair, but the MD result is very probably overestimated. The MD reorientation time for a water OH initially H-bonded to I^- leads to a value nearly identical to the bulk value; however, this MD result is obtained from a fit on the 2–10 ps time-interval during which many OHs have left the I^- shell due to the short residence time (which can be estimated from the jump time)[58] and then reorient with the bulk time. This leads to a measured reorientation time very similar to the bulk.

Table 3 Various quantities associated with the Extended Jump Model

	F^-	I^-	H_2O
τ_2/ps[a]	6.1	3.3[b]	3.4
$\langle\tau_2^{\mathrm{EJM}}\rangle_{\Delta\theta}$/ps	6.2	2.5	3.3
τ_2^{EJM} ($\langle\Delta\theta\rangle$)/ps	5.7	2.2	2.9
τ_2^{jump}/ps[c]	18.1	3.3	5.1
τ_{frame}/ps	9.5	9.3	9.5
τ_{jump}/ps	12.2	3.0	4.0
$\tau^{\mathrm{jump}}/\tau_{\mathrm{bulk}}^{\mathrm{jump}}$	3.1	0.8	1.0
$\langle\Delta\theta\rangle$/°	63.0	73.0	68.0

[a] Computed from the exponential tail of MD $C_2(t)$. [b] Because the residence time[58] of water next to I^- is short compared to the 2–10 ps time range used for the exponential fit of $C_2(t)$, this τ_2 value contains a non-negligible contribution from the reorientation of waters which have already left the I^- hydration shell and should thus be considered as an upper bound. [c] Contribution to the reorientation time coming exclusively from the jumps; it corresponds to the first term in eqn (4).

Table 4 Ratios ρ of the reorientation times τ_2 with their bulk water reference values

	F^-	I^-	H_2O
ρ_2[a]	1.8	1.0[b]	1.0
ρ_2^{EJM} ($\langle\Delta\theta\rangle$)	1.9	0.8	1.0
$\langle\rho_2^{\mathrm{EJM}}\rangle_{\Delta\theta}$	1.9	0.7	1.0
$\rho_2^{^1\mathrm{H\ NMR}}(H_2O)$[8]	2.3	0.5	1.0
$\rho_2^{^1\mathrm{H\ NMR}}(D_2O)$[42]	2.72	0.38	1.0
$\rho_2^{^{17}\mathrm{O\ NMR}}(D_2O)$[42]	2.8	0.46	1.0

[a] Computed from the exponential tail of the MD $C_2(t)$. [b] Because the residence time[58] of water next to I^- is short compared to the 2–10 ps time range used for the exponential fit of $C_2(t)$, this τ_2 value contains a non-negligible contribution from the reorientation of waters which have already left the I^- hydration shell and should thus be considered as an upper bound.

The EJM prediction is probably a better estimate in this case since it is based on the jump time, which is defined with absorbing boundary conditions in the new H-bonded state.

We now turn to the structuring or de-structuring characters of the two ions, evaluated through the slowdown factors comparing each anion's first hydration shell water reorientation time to the neat water value, *i.e.* the ratio of τ_2 values. The results are detailed in Table 4. For the F^- anion, the strong structure-making dynamic character is clearly indicated by the direct simulation, EJM and NMR experimental results. The results for the weaker H-bonding, lower charge density I^- anion are less consistent in their magnitude, but generally indicate a structure-breaking character, whose degree is greater for the NMR experimental results than for either the direct simulation or the EJM results (for the former, footnote b of Table 4 should be consulted).

The EJM component predictions in Table 3 are very instructive concerning the distinct character of the F^- anion compared to I^- and neat water. For the latter two cases, the faster τ_2^{jump} jump contribution to τ_2—reflecting the small time τ_{jump} value in Tables 2 and 3—is dominant. In striking contrast, for the F^- first hydration shell water reorientation, it is the faster frame reorientation that is more important for τ_2; the strong $F^-\cdots H_2O$ H-bond leads to a large jump time τ_{jump} in Tables 2 and 3, *i.e.* a small rate constant for the H-bond partner exchange, which is reflected in the smaller jump contribution in Table 2. Although not investigated here, this same dominance of the frame reorientation component might be expected for sufficiently small multiply charged anions (and cations) with large residence times for the first hydration shell water molecules.

We have noted at the end of Section 3 that there is a distortion in the fsIR determination of τ_2 related to the population lifetime T_1 of the water OH vibration whose orientation is probed.[18] Briefly, monitoring of the OH orientation in these experiments depends on the vibrational lifetime T_1 for water in the first hydration shell of the anion being longer than T_1 for a bulk water molecule in order to distinguish the former situation from the latter. For the case of Cl^-, this introduces a bias in favor of an intact $Cl^-\cdots H_2O$ H-bonded pair, whose reorientational dynamics is governed by the slower time τ_{frame} rather than by eqn (2), which is

dominated by the faster jump contribution in eqn (4) and not by τ_{frame}.[18] Following the same analysis as in ref. 18 and employing the population lifetime values given in ref. 59, this same effect is visible for the I^- case in Table 2: the MD reorientation time determined including the lifetime effect—which is close to the time determined in the fsIR experiment[30]—is more than double the MD time determined from the $C_2(t)$ tcf. In addition, we note that the high salt concentration used in the fsIR experiments[30] (3 M NaI) is expected to lead to a further slowdown in the water dynamics compared to our simulated system which is a single dilute anion in water. Such salt concentration-induced slowdown has already been shown in previous simulations.[18]

In the EJM, which we have shown to give a good account of the anionic hydration shell reorientation times, the jump time τ_{jump} (defined as the inverse of the H-bond partner exchange rate constant for the reorienting water OH) played a role which is dominant for I^- and important, though not dominant, for F^-. As we indicated above, this feature is associated with the strong $F^-\cdots H_2O$ H-bond, which lengthens τ_{jump} compared to the more weakly bonded $I^-\cdots H_2O$ situation, reducing the jump's importance in determining τ_2 *via* eqn (4).

This effect on the exchange rate constant can be comprehended within the EJM by noting that the reorientation arises from the concerted breaking of the initial H-bond and making of the final H-bond. We restrict our attention to the slowdown/acceleration factor $\rho_{jump} = \tau_{jump}^{X^-}/\tau_{jump}^{H_2O}$ for the anion X^- compared to the bulk water situation. Since the final acceptor (a water oxygen) is the same in each case, ρ_{jump} is determined by[27] the difference, referenced to an initial water H-bond acceptor, in the activation free energy contribution to reach the exchange transition state starting from the initial H-bond acceptor, the anion $X^- = F^-$ or I^- in our case. Inspection of the ion-water radial distribution functions in Fig. 1 shows that the great slowdown next to F^- compared to the bulk case originates from the stronger H-bond with F^- while the acceleration next to I^- comes from the weak H-bond with I^- which facilitates the elongation of this initial H-bond during the jump reorientation.

5. Concluding remarks

We have described the Molecular Dynamics (MD) simulation and theoretical description of water reorientation in the first hydration layer of the fluoride and iodide ions, as limiting cases in the (standard) halide anion series. The MD results are in general accord with NMR experimental results, in particular with NMR *B* factors, and from a dynamical perspective, they characterize F^- as a strong structure-maker and I^- as a weak structure-breaker. For both anions, the reorientation mechanism involves contributions from sudden and large amplitude jumps from one hydrogen (H) bonding partner to another, and from the reorientation of the axis of an intact anion–water H-bonded pair, whose contributions to the water reorientation time are well described by the Extended Jump Model (EJM). Due to its strong H-bond with water, F^- exhibits the unusual behavior of having its reorientation dominated by the axis rotation, although the jump component remains important. By contrast, the jump component is dominant for the case of the relatively weak $I^-\cdots H_2O$ H-bond. This H-bonding strength disparity also impacts the jump rate constant. It was noted that the dominance of the frame reorientation is expected to also be found for multiply charged ions with sufficiently long residence times for the first hydration shell water molecules.

One among several extensions and applications of the present work would be to examine the reorientational dynamics of these and other anions at aqueous interfaces, since the hydration water reorientation dynamics can be involved in *e.g.* interfacial reactions,[60,61] and should differ from that in bulk aqueous ionic solution.

Acknowledgements

We thank Fabio Sterpone (IBPC, Paris) for his comments. This work was supported in part by a doctoral fellowship from UPMC Paris Universitas ED388 (JB) and by NSF grant CHE-0750477 (JTH).

References

1 H. Ohtaki and T. Radnai, *Chem. Rev.*, 1993, **93**, 1157–1204.
2 Y. Marcus, *Chem. Rev.*, 2009, **109**, 1346–1370.
3 B. J. Gertner, R. M. Whitnell, K. R. Wilson and J. T. Hynes, *J. Am. Chem. Soc.*, 1991, **113**, 74–87.
4 K. Ando and J. T. Hynes, *J. Phys. Chem. B*, 1997, **101**, 10464–10478.
5 R. Bianco and J. T. Hynes, *J. Phys. Chem. A*, 2003, **107**, 5253–5257.
6 R. Bianco and J. T. Hynes, *J. Phys. Chem. A*, 1999, **103**, 3797–3801.
7 C. D. Taylor and M. Neurock, *Curr. Opin. Solid State Mater. Sci.*, 2005, **9**, 49–65.
8 L. Endom, H. G. Hertz, B. Thul and M. D. Zeidler, *Ber. Bunsen-Ges.*, 1967, **71**, 1008–1031.
9 G. Engel and H. G. Hertz, *Ber. Bunsen-Ges.*, 1968, **72**, 808–834.
10 K. Yoshida, K. Ibuki and M. Ueno, *J. Solution Chem.*, 1996, **25**, 435–453.
11 H. J. Bakker, *Chem. Rev.*, 2008, **108**, 1456–1473.
12 D. E. Moilanen, D. Wong, D. E. Rosenfeld, E. E. Fenn and M. D. Fayer, *Proc. Natl. Acad. Sci. U. S. A.*, 2009, **106**, 375–380.
13 S. Park and M. D. Fayer, *Proc. Natl. Acad. Sci. U. S. A.*, 2007, **104**, 16731–16738.
14 M. B. Ji, M. Odelius and K. J. Gaffney, *Science*, 2010, **328**, 1003–1005.
15 S. Park, M. Odelius and K. J. Gaffney, *J. Phys. Chem. B*, 2009, **113**, 7825–7835.
16 I. A. Heisler and S. R. Meech, *Science*, 2010, **327**, 857–860.
17 D. A. Schmidt, O. Birer, S. Funkner, B. P. Born, R. Gnanasekaran, G. W. Schwaab, D. M. Leitner and M. Havenith, *J. Am. Chem. Soc.*, 2009, **131**, 18512–18517.
18 D. Laage and J. T. Hynes, *Proc. Natl. Acad. Sci. U. S. A.*, 2007, **104**, 11167–11172.
19 Some aspects of simulated water reorientation for the Bromide ion case are given in ref. 20.
20 Y. S. Lin, B. M. Auer and J. L. Skinner, *J. Chem. Phys.*, 2009, **131**, 144511.
21 A. K. Soper and K. Weckstrom, *Biophys. Chem.*, 2006, **124**, 180–191.
22 R. Mancinelli, A. Botti, F. Bruni, M. A. Ricci and A. K. Soper, *Phys. Chem. Chem. Phys.*, 2007, **9**, 2959–2967.
23 D. Laage and J. T. Hynes, *Science*, 2006, **311**, 832–835.
24 D. Laage and J. T. Hynes, *J. Phys. Chem. B*, 2008, **112**, 14230–14242.
25 D. Laage, G. Stirnemann and J. T. Hynes, *J. Phys. Chem. B*, 2009, **113**, 2428–2435.
26 G. Stirnemann, P. J. Rossky, J. T. Hynes and D. Laage, *Faraday Discuss.*, 2010, **146**, 263–281.

27 F. Sterpone, G. Stirnemann, J. T. Hynes and D. Laage, *J. Phys. Chem. B*, 2010, **114**, 2083–2089.
28 G. Stirnemann, J. T. Hynes and D. Laage, *J. Phys. Chem. B*, 2010, **114**, 3052–3059.
29 P. L. Geissler, J. D. Smith and R. J. Saykally, *J. Am. Chem. Soc.*, 2007, **129**, 13847–13856.
30 M. F. Kropman, H. K. Nienhuys and H. J. Bakker, *Phys. Rev. Lett.*, 2002, **88**, 77601.
31 A. Tongraar and B. M. Rode, *Phys. Chem. Chem. Phys.*, 2003, **5**, 357–362.
32 J. M. Heuft and E. J. Meijer, *J. Chem. Phys.*, 2005, **123**, 094506.
33 S. Chowdhuri and A. Chandra, *J. Phys. Chem. B*, 2006, **110**, 9674–9680.
34 A. Tongraar, S. Hannongbua and B. M. Rode, *J. Phys. Chem. A*, 2010, **114**, 4334–4339.
35 P. Jungwirth and D. J. Tobias, *J. Phys. Chem. B*, 2002, **106**, 6361–6373.
36 H. F. Xu, H. A. Stern and B. J. Berne, *J. Phys. Chem. B*, 2002, **106**, 2054–2060.
37 A. Grossfield, P. Y. Ren and J. W. Ponder, *J. Am. Chem. Soc.*, 2003, **125**, 15671–15682.
38 J. W. Ponder, C. J. Wu, P. Y. Ren, V. S. Pande, J. D. Chodera, M. J. Schnieders, I. Haque, D. L. Mobley, D. S. Lambrecht, R. A. DiStasio, M. Head-Gordon, G. N. I. Clark, M. E. Johnson and T. Head-Gordon, *J. Phys. Chem. B*, 2010, **114**, 2549–2564.
39 D. A. Case, T. A. Darden, T. E. Cheatham III, C. L. Simmerling, J. Wang, R. E. Duke, R. Luo, M. Crowley, R. C. Walker, W. Zhang, K. M. Merz, B. Wang, S. Hayik, A. Roitberg, G. Seabra, I. Kolossvary, K. F. Wong, F. Paesani, J. Vanicek, X. Wu, S. R. Brozell, T. Steinbrecher, H. Golhlke, L. Yang, C. Tan, J. Mongan, V. Hornak, G. Cui, D. H. Mathews, M. G. Steetin, C. Sagui, V. Babin and P. A. Kollman, *AMBER 10*, University of California, San Francisco, 2008.
40 D. Frenkel and B. Smit, *Understanding Molecular Simulation. From Algorithms to Applications*, Academic Press, San Diego, 2002.
41 T. S. Hofer, H. T. Tran, C. F. Schwenk and B. M. Rode, *J. Comput. Chem.*, 2004, **25**, 211–217.
42 A. Shimizu and Y. Taniguchi, *Bull. Chem. Soc. Jpn.*, 1991, **64**, 1613–1617.
43 A. Abragam, *The Principles of Nuclear Magnetism*, Clarendon, Oxford, UK, 1961.
44 J. Jonas, T. Defried and D. J. Wilbur, *J. Chem. Phys.*, 1976, **65**, 582–588.
45 E. Lang and H. D. Ludemann, *J. Chem. Phys.*, 1977, **67**, 718–723.
46 B. Halle and J. Qvist, *J. Am. Chem. Soc.*, 2008, **130**, 10345–10353.
47 J. Ropp, C. Lawrence, T. C. Farrar and J. L. Skinner, *J. Am. Chem. Soc.*, 2001, **123**, 8047–8052.
48 Y. Ishihara, S. Okouchi and H. Uedaira, *J. Chem. Soc., Faraday Trans.*, 1997, **93**, 3337–3342.
49 H. G. Hertz and M. D. Zeidler, *Ber. Bunsen-Ges.*, 1964, **68**, 821–837.
50 J. R. C. Vandermaarel, D. Lankhorst, J. Debleijser and J. C. Leyte, *J. Phys. Chem.*, 1986, **90**, 1470–1478.
51 A. Bagno, F. Rastrelli and G. Saielli, *Prog. Nucl. Magn. Reson. Spectrosc.*, 2005, **47**, 41–93.
52 R. Ludwig, F. Weinhold and T. C. Farrar, *J. Chem. Phys.*, 1995, **103**, 6941–6950.
53 Y. L. A. Rezus and H. J. Bakker, *J. Chem. Phys.*, 2005, **123**, 114502.
54 D. Laage, G. Stinermann, F. Sterpone, R. Rey and J. T. Hynes, *Annu. Rev. Phys. Chem.*, 2011, **62**, 395–416.
55 D. Laage, G. Stirnemann, F. Sterpone and J. T. Hynes, *Acc. Chem. Res.*, 2011, DOI: 10.1021/ar200075u, in press.
56 E. N. Ivanov, *Sov. Phys. JETP*, 1964, **18**, 1041–1045.
57 S. H. Northrup and J. T. Hynes, *J. Chem. Phys.*, 1980, **73**, 2700–2714.
58 D. Laage and J. T. Hynes, *J. Phys. Chem. B*, 2008, **112**, 7697–7701.
59 M. F. Kropman and H. J. Bakker, *J. Chem. Phys.*, 2001, **115**, 8942–8948.
60 R. Bianco and J. T. Hynes, *Acc. Chem. Res.*, 2006, **39**, 159–165.
61 M. Roeselova, P. Jungwirth, D. J. Tobias and R. B. Gerber, *J. Phys. Chem. B*, 2003, **107**, 12690–12699.